Adsorption (2014) 20:889–897
DOI 10.1007/s10450-014-9632-x

Adsorption of argon on mesoporous anodic alumina

Lorenzo Bruschi · Giampaolo Mistura · Sang-Joon Park · Woo Lee

Received: 17 June 2014 / Revised: 20 August 2014 / Accepted: 22 August 2014 / Published online: 3 September 2014

Abstract We have studied the adsorption of Ar on regular, highly-ordered alumina membranes made by anodization. The straight, non-interconnected pores have nominal diameters of 31 and 83 nm, with a relative dispersion better than 5 % in the pore size. Adsorption isotherms taken on bare membranes with pores of 83 nm present two distinct hysteresis loops. This is found to be a consequence of the fabrication procedure that yields a central circular region formed by open pores surrounded by an outer ring with closed bottom pores of smaller size, about 40 nm. For the membrane with pores of 31 nm, the difference between these pores is much smaller, about 2 nm, and this explains why the isotherms on these membranes show a single hysteresis loop as expected. Detailed real space analysis of the membranes by electron microscopy confirms the adsorption conclusions.

Keywords Adsorption isotherms · Anodic aluminum oxide (AAO) · Porous materials · Template

L. Bruschi
CNISM Unità di Padova, via Marzolo 8, 35131 Padua, Italy

G. Mistura (✉)
CNISM and Dipartimento di Fisica e Astronomia G.Galilei, Università di Padova, via Marzolo 8, 35131 Padua, Italy
e-mail: giampaolo.mistura@unipd.it

S.-J. Park · W. Lee (✉)
Korea Research Institute of Standards and Science (KRISS), Yuseong, Daejeon 305–340, Korea
e-mail: woolee@kriss.re.kr

W. Lee
Korea University of Science and Technology (KUST), Yuseong, Daejeon 305–333, Korea

1 Introduction

Self–assembled porous materials with hierarchical porous nanostructures are of tremendous importance in nanoscience and nanotechnology (Hoa et al. 2006; Stein 2003; Lee et al. 2008). Examples of such materials include nanospheres (artificial opals and inverse opals) (Zakhidov et al. 1998; Xia et al. 2000; Stein 2001), silica SBA-15 (Zhao et al. 1998; Zhao et al. 1998; Kruk et al. 2000; Kruk and Jaroniec 2011) and MCM-41 (Beck et al. 1992; Ying et al. 1998; Asefa et al. 1999), block copolymers (Zhao et al. 1998; Xia et al. 1999; Bang et al. 2006) and porous alumina containing hexagonal arrays of cylindrical pores (Lee et al. 2006; Lee and Kim 2010; Lee et al. 2008; Masuda and Fukuda 1995; Lee and Park 2014). A crucial step in the practical applications of these porous materials regards the accurate evaluation of the size, length and internal structure of the pores. This is especially important during the development stages of a new methodology and in the final validation of its products. Such a task is generally achieved by taking extensive micrographs with a scanning electron microscope (SEM) or, for the smallest scales, with a transmission electron microscope (TEM). However, these techniques present some limitations in the study of porous structures. In particular, (a) the examined area is a tiny fraction of that of the sample and there is always the problem of the validity of such results to the whole sample, (b) their absolute peak positions depend to a large extent on the imaging conditions and the thresholding procedure, (c) the sample must be broken to look at the pore morphology. The determination of adsorption isotherms allows to overcome some of these limitations and provides quantitative data about the pores morphology.

Here we present a comprehensive adsorption and SEM study of porous alumina aimed at fabricating very uniform

and well characterized membranes to be used for the spatial confinement of fluids. In the next section we discuss the anodization procedure developed to make the porous membranes, with a particular attention to the opening of the bottom aluminum barrier. After a brief description of the torsional microbalance used for the adsorption measurements, we will present and discuss the main results. In particular, we find that the barrier layer opening and subsequent pore widening treatment in the central region of the samples leaves out an outer ring where the pores have closed bottom ends and smaller size and the difference in pores size in these two regions is dependent on the time for pore widening.

2 Experimental

2.1 Sample preparation

Porous anodic aluminum oxide (AAO) samples employed in the present study were prepared by anodization of aluminum. In brief, as-received Al disks (2 cm in diameter, Goodfellow, 99.999 %) were used in anodization experiments without the annealing step. The Al disks were electrochemically polished in a vigorously stirred 1:4 mixture solution of 65 % $HClO_4$ and 99.5 % ethanol (5 °C) in order to exclude the effects (e.g., localized field concentration) that could arise from the surface roughness during the anodization. The finished Al disc was placed in an electrochemical cell with an O-ring (diameter = 1.5 cm), so that one side of metal can be anodized. All anodization experiments in the present work were performed by using an electrochemical cell equipped with a cooling stage which is in thermal contact with the Al substrate to remove the reaction heat (Lee et al. 2006; Lee and Kim 2010). Mirror finished Al discs were then potentiostatically anodized for 24 h by using either 0.3 M $H_2C_2O_4$ (1 °C) at 40 V or 0.3 M H_2SO_4 (1 °C) at 25 V for the preparation of AAOs with different pore sizes (D_p) and densities (n). The anodized Al was then immersed into a mixed solution of 1.8 wt% CrO_3 and 6 wt% H_3PO_4 at 45 °C for 12 h to remove the oxide layer with disordered pore structure. Next, the resulting Al substrate with highly ordered arrays of approximately hemispherical concavities was anodized under the same conditions as the first anodization for the desired period of time (typically 6 to 12 h). Each concavity on the surface of the Al substrate serves as pore initiation site during the second anodization process. According to our field emission scanning electron microscopy (FESEM, Hitachi S-4800) analysis, the average pore diameter (D_p), interpore distance (D_{int}), and pore density (n) of AAOs were determined to be $D_p = 30$ nm, $D_{int} = 105$ nm, and $n = 1.05 \times 10^{10}$ pores/cm^2 for AAOs formed by using 0.3 M $H_2C_2O_4$ (i.e., $H_2C_2O_4$-AAOs), while

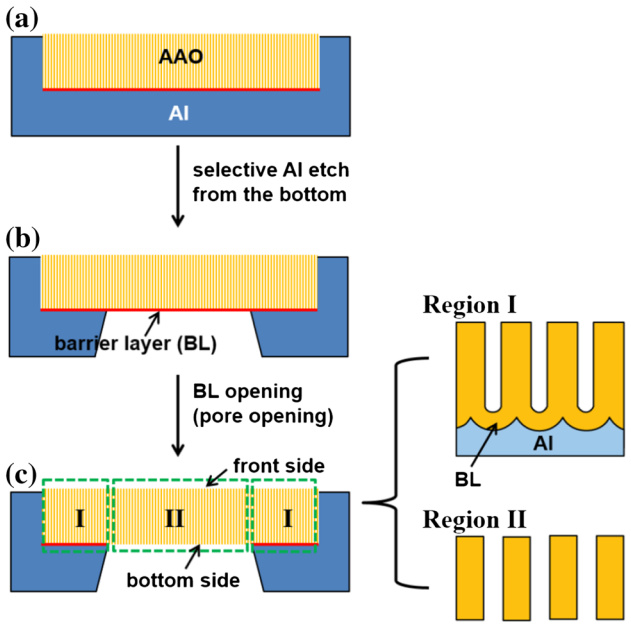

Fig. 1 Schematic procedure of preparation of Open samples: **a** as-prepared AAO, **b** after selective backside etching of Al substrate, and **c** after removal of barrier layer (BL, *red lines*). Regions I and II refer respectively to the outer ring comprised of *closed bottom pores* and the central area with *open bottom pores*. The sample has the shape of a disk of diameter D = 2 cm and the width of the ring corresponding to region I is about a couple of mm (Color figure online)

$D_p = 22$ nm, $D_{int} = 60$ nm, and $n = 2.73 \times 10^{10}$ pores/cm^2 for AAOs formed by using 0.3 M H_2SO_4 (H_2SO_4-AAOs). In the anodization of aluminum under given electrochemical conditions, the thickness (t_p) of the resulting AAO (*i.e.*, the length of nanopores) is linearly proportional to the total amount of charge involved in the electrochemical oxidation. Therefore, one may precisely control the thickness of AAO by adjusting the anodization time. With our anodization conditions, the thickness of AAO formed after 6 h of anodization was found to be $t_p = 26.8$ and 35.8 μm for $H_2C_2O_4$ and H_2SO_4 anodization, respectively.

Pore bottom of an as-prepared AAO sample is closed by the thin barrier oxide layer that is in conformal contact with the underlying Al substrate. As schematically shown in Fig. 1, through-hole AAO membranes were prepared by selective removal of the underlying Al substrate by using a mixture solution containing 3.4 g of $CuCl_2 \cdot H_2O$, 50 mL of 37 wt% HCl, and 100 mL of DI water, followed by opening of the barrier layer by using 5 wt% H_3PO_4 solution (30 °C). In order to prevent undesired widening of AAO pores by the etchant solutions used for the removal of the Al substrate and the barrier layer, the central region of the backside of the anodized sample was selectively exposed to the etchant solutions, which could be achieved by placing the sample in an electrochemical cell with an O-ring (Diameter = 1.0 cm). According to our SEM investigation,

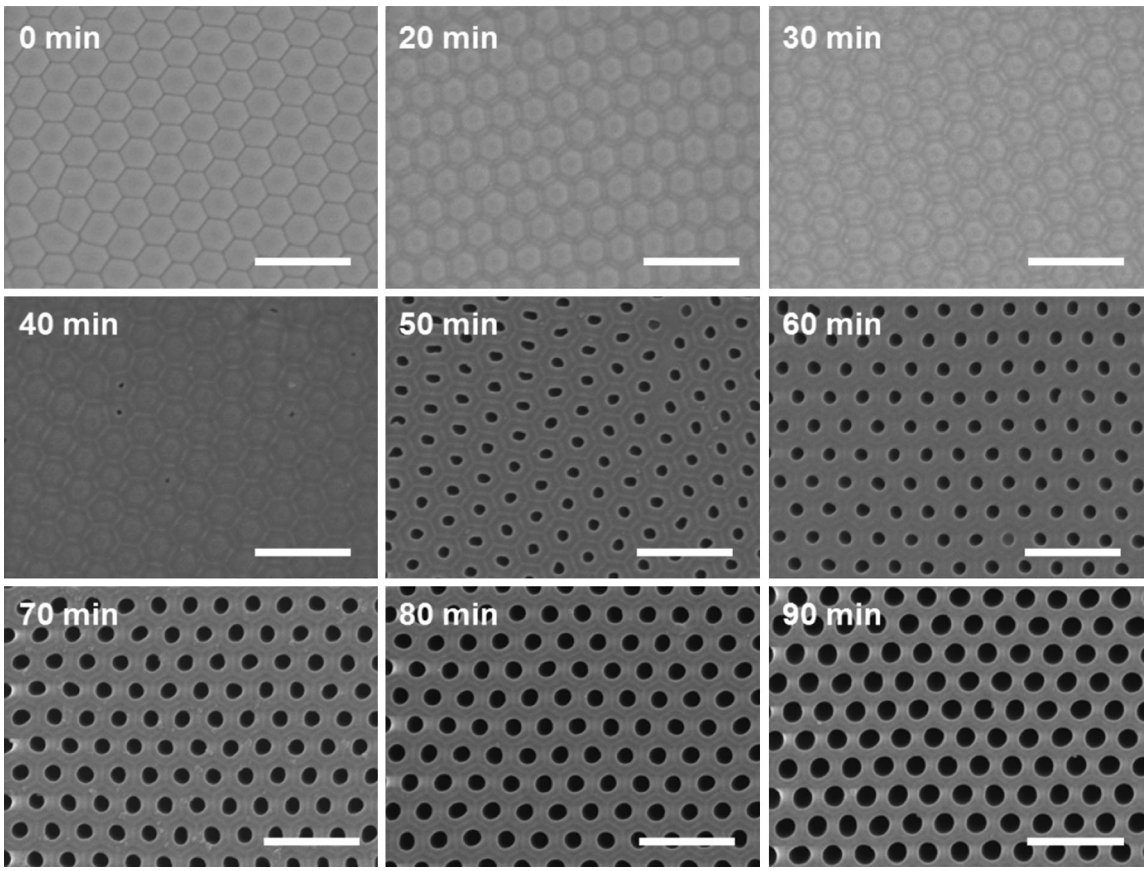

Fig. 2 Representative SEM images showing the evolution of the barrier layer morphology as a function of etching time. Etching of the barrier layer of $H_2C_2O_4$-formed AAO was performed by using 5 wt% H_3PO_4 at 30 °C. The *scale bars* correspond to 300 nm

opening of the barrier layer took place after 40 min under the present processing conditions (see Fig. 2). Actually, the removal of the barrier layer at the bottom of pores is a crucial step in the preparation of AAO membranes. By performing in situ electrochemical measurements using a pair of electrodes across an AAO sample, we know exactly when the pores are starting to open(Han et al. 2013). However, the complete opening of the pores requires systematic calibrations of the etching times accompanied by an investigation of the pore bottom morphology.

In order to investigate the effect of pore size on adsorption, pores of $H_2C_2O_4$-AAO membranes were widened by immersing the as-prepared sample in a 5 wt% H_3PO_4 solution (30 °C) for desired periods of time. This pore widening treatment increased the pore size from 30 to 83 nm after an immersion time of 50 min. For H_2SO_4-AAO membranes, on the other hand, we did not perform the pore widening process. According to our SEM image analysis based on standard image processing software (i.e., Image J) (Rasband et al. 2006), the pore size difference between the top and bottom pores turned out to be less than 1.5 % for $H_2C_2O_4$-AAOs and 5 % for H_2SO_4-AAOs. These differences in both types of AAO samples can be attributed to the detailed compositional nature of pore wall oxides (Lee and Park 2014; Han et al. 2013). Throughout this paper, AAO samples with closed bottom end will be denoted as "Closed", while AAO samples with pores open at both ends as "Open".

2.2 Adsorption measurement

Adsorption isotherms have been measured with a torsional microbalance (Bruschi et al. 2001, 2003). The porous samples, having a characteristic size of $\sim$2 cm and a thickness of a few hundred microns, were attached to the extremity of a tungsten rod driven to its torsional frequency. As the samples were exposed to a vapor of Argon at $T = 85$ K, the resonance frequency decreased because of an increase in the total moment of inertia. From the vapor corrected frequency shifts it was then possible to derive the relative change of the oscillator moment of inertia, which is proportional to the mass of the adsorbed film (Bruschi et al. 2001, 2003). With this microbalance it is possible to measure the adsorption on thin solid substrates of different shapes (e.g., square, rectangular, circular etc.) having a typical size of about 1 cm and thickness less than 1 mm. For porous substrates, its

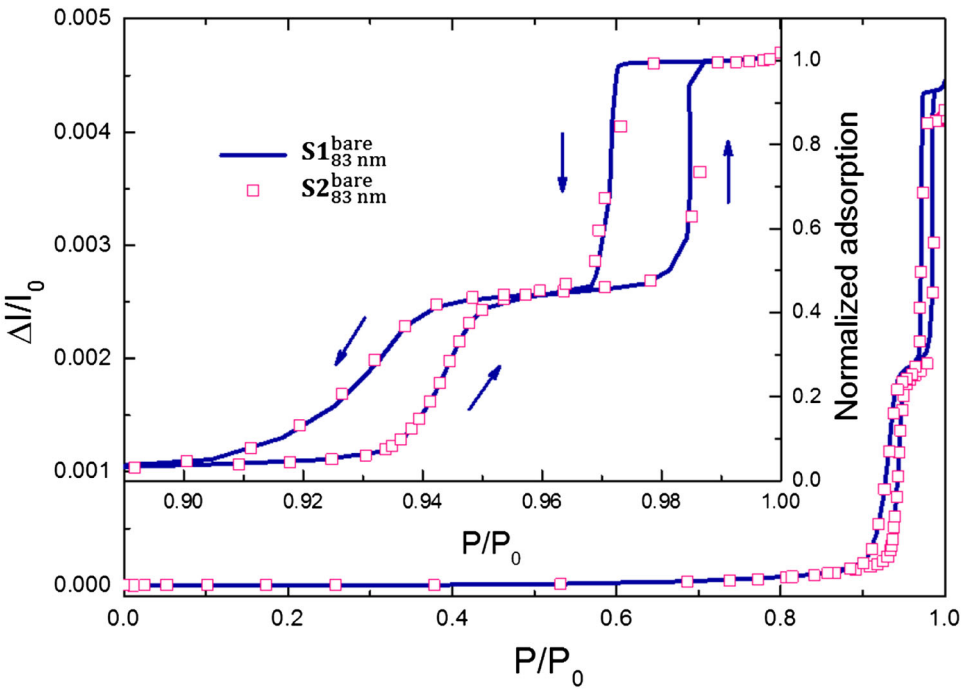

Fig. 3 Adsorption isotherms of Ar at $T = 85$ K on two bare Open alumina samples of nominal pore diameter $D_P = 83$ nm, ($S1^{bare}_{83nm}$ and $S2^{bare}_{83nm}$). The size D_P refers to the pores in the central part of the samples, e.g. region II. Inset shows the enlargement of their final part close to saturation. *Arrows* indicate the adorption (gas is added) and desorption (gas is removed) branches

sensitivity amounts to a small fraction of an adsorbed monolayer.

3 Results and analysis

Figure 3 shows two adsorption isotherms of argon taken on different Open samples having the same nominal size $D_p = 83$ nm, where D_p refers to the pores in the central part of the samples, e.g. region II. The samples are labeled $S1^{bare}_{83nm}$ and $S2^{bare}_{83nm}$, where the upscript "bare" refers to the fact that for these measurements no epoxy has been used to selectively block the pores ends. These curves represent the relative change of the oscillator moment of inertia, $\Delta I/I_0$, as a function of relative pressure, P/P_0, where $P_0 = 65$ kPa is the bulk saturating vapor pressure for Ar at 85 K. At low pressure they present no adsorption, but this is only an artifact of the analysis method. Actually, the decrease in the microbalance frequency due to viscous coupling is determined by fitting the data at low relative pressures $P/P_0 \leq 0.2$ under the assumption that, in this region, the adsorption contribution is negligible. At $P/P_0 > 0.9$ a very steep and large step occurs (mid-point position $P_{mid\text{-}point}/P_0 = 0.943$), followed by a plateau, a second step ($P_{mid\text{-}point}/P_0 = 0.985$) and a new rise very close to saturation due to condensation of a thick film on the two faces of the AAO disk.

To facilitate their comparison, the inset displays the same data in much enlarged scale close to saturation and the adsorption data have been normalized to the value of the plateau observed before condensation. The two resulting curves overlap nicely suggesting a good control in the sample fabrication. The isotherms are characterized by two pronounced hysteresis loops formed during gas addition (adsorption) and removal (desorption) from the sample cell. Their shape resembles that of type H1 in the IUPAC classification (Sing et al. 1985) (e.g., a hysteresis loop with parallel adsorption and desorption branches), which is generally associated to capillary condensation and evaporation in ordered mesoporous materials with cylindrical pores open at both ends. For instance, type H1 loops are observed not only in porous alumina (Bruschi et al. 2008; Casanova et al. 2008) but also in ordered mesoporous silicas like SBA and MCM-41 (Esparza et al. 2004; Grosman and Ortega 2005; Morishige and Ito 2002). At variance with standard isotherms, the curves in Fig. 3 present two pronounced and distinct loops, which resemble those observed in porous Si duplex layers (Grosmann and Ortega 2011; Casanova et al. 2012).

To understand their origin, we have selectively blocked the pore openings at the front side by painting with a soft brush a thin layer of Loctite® Super Glue, a fast bonding, instant adhesive in a very humid environment for a very rapid cure. Then, the glue is covered with Stycast® 2850 FT (Emerson and Cuming), a two-component epoxy resin used in cryogenics because of its good thermal conductivity and low coefficient of thermal expansion. The use of the fast-curing glue avoids that the pores get filled by the liquid adhesive by capillarity. The epoxy is instead necessary to guarantee the mechanical integrity of the sample

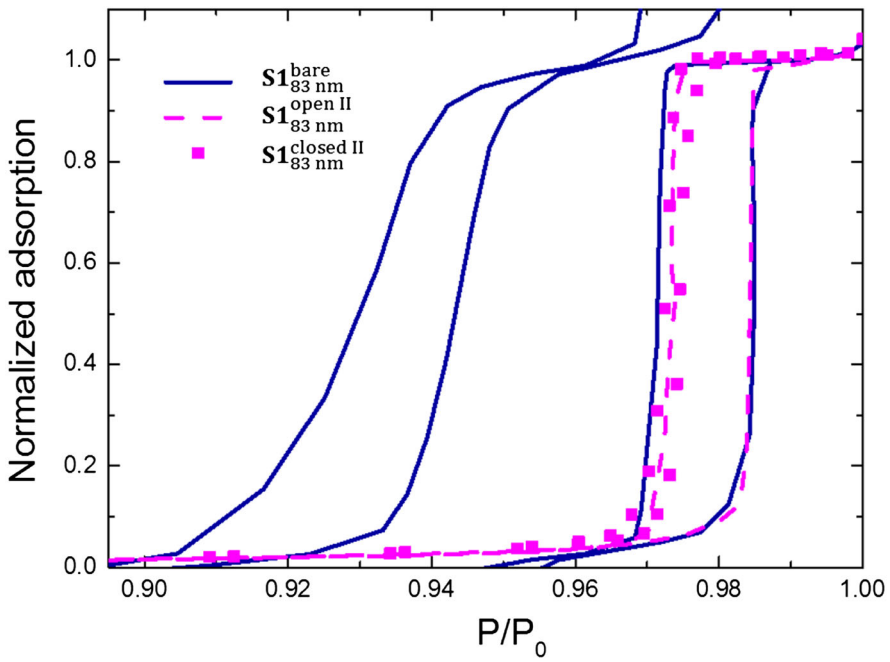

Fig. 4 Final portion of the adsorption isotherm taken on bare Open alumina ($S1^{bare}_{83nm}$) where the two subloops have been vertically shifted and rescaled and of isotherms on epoxied Open alumina. $S1^{openII}_{83nm}$: hysteresis loop the open pores in the central area, Region II. $S1^{closedII}_{83nm}$: hysteresis loop after closure of the bottom pores in Region II

during the cool down to 85 K, otherwise it will crack because of the large thermal contraction of the glue (see Bruschi et al. 2014 for further details).

Figure 4 compares the hysteresis loops of the epoxied samples with those found on the bare substrates. In both epoxied samples, the mouths of the closed bottom pores of the outer ring (Region I of the cartoon of Fig. 1) have been blocked so that only the pores in the central area were exposed to Ar. The (blue) continuous line indicates the two loops after they have been vertically shifted and rescaled so that each one spans the interval of normalized adsorption comprised between 0 and 1. The (magenta) dashed line represents the isotherm of the epoxied sample presenting open pores in the central area (Region II) labelled as $S1^{openII}_{83nm}$. The very close agreement with the rescaled second loop suggests that this latter one is due to the adsorption on the open pores of the central area. Actually, assuming pores of cylindrical shape, we have analyzed the position of the evaporation branches of Fig. 4 in terms of the classical Kelvin equation of capillary condensation (Evans et al. 1986; Bruschi and Mistura 2009):

$$ln\frac{P_{evap}}{P_0} = -\frac{\gamma}{n_l K_B T}\frac{4}{D_P} \quad (1)$$

where $\gamma = 13.1$ erg/cm^2 is the liquid argon surface tension and $n_l = 2.1 \times 10^{22}$ atoms/cc is the liquid argon number density both evaluated at the temperature $T = 85$ K, $K_B = 1.38 \times 10^{-16}$ erg/K being the Boltzmann constant. According to Cohan's model (Everett 1967; Gregg and Sing 1982), in cylindrical pores the evaporation of the filling liquid proceeds through a hemispherical meniscus having a curvature $\sim \frac{4}{D_P}$. The corresponding evaporation branch occurs in the interval $P_</P_0 = 0.986 \leq P/P_0 \leq 0.992 = P_>/P_0$ with the mid-point at $P_{mid\text{-}point}/P_0 = 0.9898$. Here, $P_</P_0$ ($P_>/P_0$) corresponds to a normalized adsorption of 15 % (85 %) (Bruschi et al. 2008). This analysis yields $D_p = 78 \pm 3$ nm, where we assumed that $D_{>,<} = D_p \pm \sigma$, which is in substantial agreement with the value $D_p = 83 \pm 2$ nm derived from the real space images of the pores. Actually, if we consider the crudity of the thermodynamic model employed, this quantitative agreement is rather surprising. As expected, this simple thermodynamic analysis underestimates the pore size because it does not account for the thickness of the adsorbed layer right before condensation (Evans et al. 1986; Bruschi and Mistura 2009).

We then proceeded to block also the open mouths of the pores in the central area as well, resulting in a sample presenting only closed bottom pores in Region II,$S1^{closedII}_{83nm}$. According to the prediction of Cohan's model (Everett 1967; Gregg and Sing 1982), confirmed by density functional theory (Marconi and van Swol 1989), numerical simulations (Sarkisov and Monson 2001; Gelb 2002), mean field theory (Rascón et al. 2013), adsorption in an ideal closed bottom pore should be reversible as recently found in very ordered porous matrices made by nanolithography (Mistura et al. 2013). However, apart from this special case, all porous materials do show hysteresis regardless of the pores closures (Bruschi et al. 2014; Bruschi and Mistura 2009; Everett 1967). Actually, Fig. 4 shows that, after blocking the bottom ends of pores in Region II, the resulting hysteresis loop is found to shrink considerably

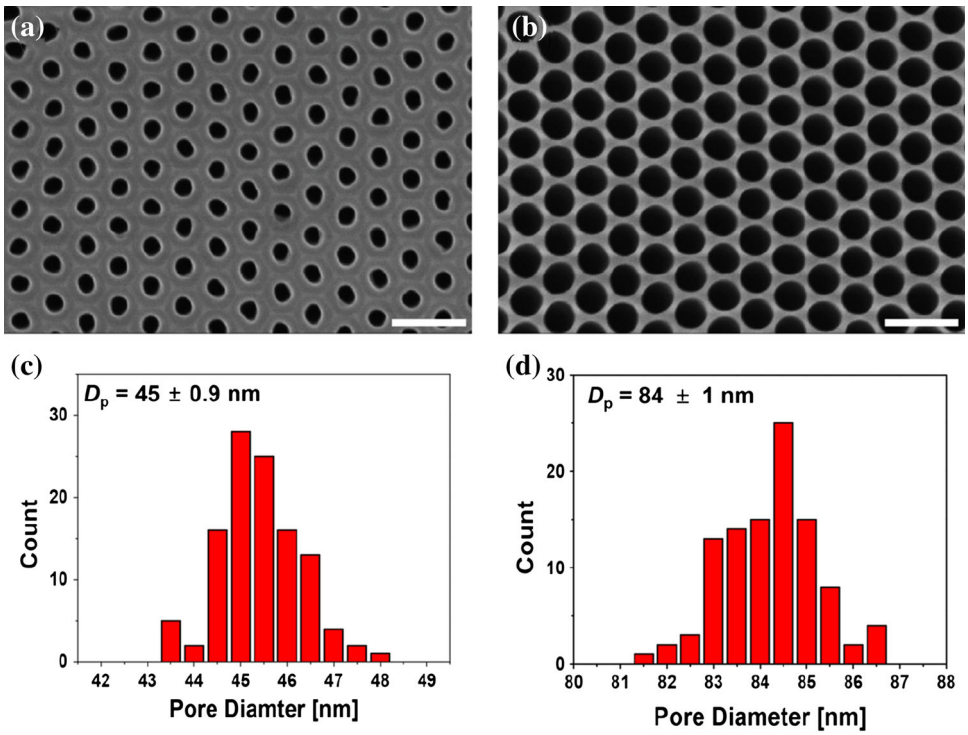

Fig. 5 Representative surface SEM images of **a** the outer ring, Region I, and **b** of the central area, Region II, of porous AAO sample $S2^{bare}_{83nm}$. The pore size distributions in the respective images are shown as histogram in **c** and **d**. *Scale bars* in (**a**) and (**b**) are 200 nm

and is centered on the desorption branch of the open pores, in full agreement with the conclusion of a systematic study on alumina pores open at one and at both ends (Bruschi et al. 2014) and numerical simulations (Fan et al. 2014; Nguyen et al. 2013). However, this loop does not agree at all with the first one observed on the Open samples. The latter one is wider, broader and located at much lower pressures. If we analyze the position of the desorption branch as done before, we get a pore size of 30 ± 4 nm.

Complementary SEM investigations confirm this finding: the measured pore sizes are $D_p = 45 \pm 0.9$ nm and 83 ± 2 nm for Region I and II, respectively (see Fig. 5). Although this technique analyzes only the pore mouths, we are confident that the distributions of Fig. 5 are representative of the pore size also inside the pores because for the sample fabrication we have employed the so-called "mild anodization" process. For this anodization condition, it is well-established that the pores are self-organized into the honeycomb-like structure and the size of pores are fairly uniform along the pore direction (i.e., from the top to the bottom of the porous membrane) (Lee and Park 2014). The axial variation in the pore size would be less than 1 %. The observed large difference in pore sizes (D_p) can be explained by the retarded diffusion of the oxide etching solution (i.e., 5wt% H_3PO_4) to the pores in Region I under geometric constraint imposed by the cell used for the barrier layer opening and subsequent pore widening treatment for an extended period of time (i.e., 50 min). Since the barrier layer in Region I is protected by the underlying Al substrate, widening of pores in this area can occur only by the etchant diffused from Region II. However, this diffusion is greatly hindered because pores at the front surface come in contact with the cell base, resulting in retarded pore wall etching at Region I. Accordingly, the difference in the pore sizes in the regions I and II is dependent on the time for pore widening.

We have repeated this sequence of measurements on different porous AAO samples with smaller nominal size, $D_p = 31$ nm. Figure 6 shows the isotherm measured on the bare membrane S^{bare}_{31nm}. At variance with the $D_p = 83$ nm pores, it presents only one hysteresis loop which is located at a lower relative pressures because the pores are smaller than in Fig. 3. To better understand its shape, we compare it with the isotherms taken after selective closures of the pores with epoxy. The isotherm corresponding to adsorption only on the closed bottom pores of region II, $S^{closedII}_{31nm}$, presents a loop which is shifted to higher relative pressure and the relative change in the moment of inertia is smaller by a factor of 10 with respect to the bare sample. The complementary isotherm relative to adsorption only on the closed bottom pores of region I, $S^{closedI}_{31nm}$, is instead shifted to lower pressures and $\Delta I/I_0$ is larger than the previous one. The difference in $\Delta I/I_0$ reflects the geometric contribution of the two regions. If a uniform distribution of equal pores is assumed in the two regions, e.g. a central disk of radius $r_1 \sim 5$ mm and an outer circular ring delimited by r_1 and $r_2 \sim 7.8$ mm, then $(\Delta I/I_0)_I/(\Delta I/I_0)_{II} \sim \left(r_2^4 - r_1^4\right)/r_1^4 \sim 4.9$, reasonably close to the ratio ~4.3 between the plateaus of two isotherms.

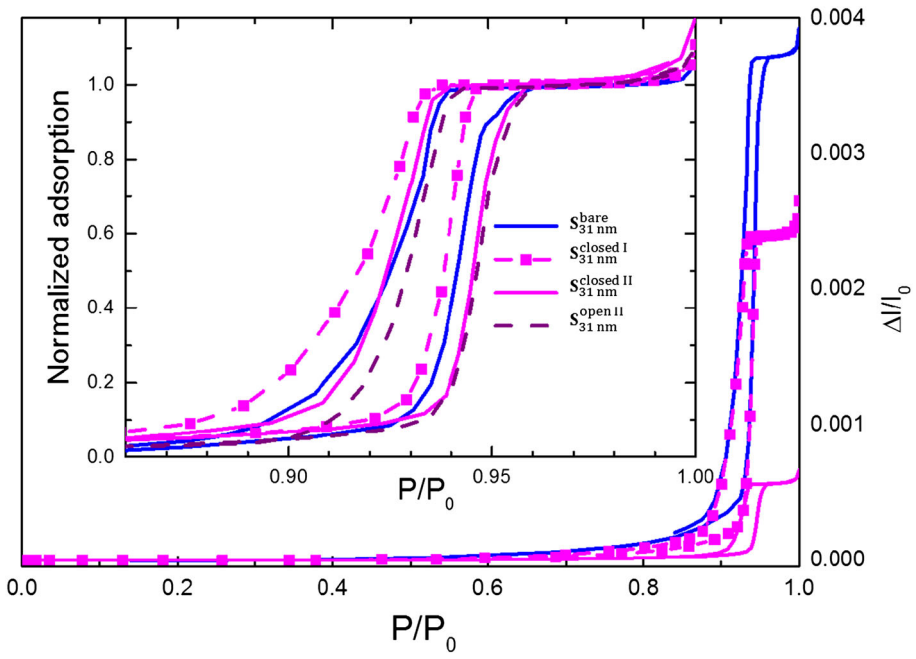

Fig. 6 Adsorption isotherms of Ar at $T = 85$ K on alumina samples of nominal diameter $D_P = 31$ nm (the size D_P refers to the pores in the central part of the samples, e.g. region II). S^{bare}_{31nm}: isotherm of the bare membrane. $S^{closedI}_{31nm}$: isotherm of the closed bottom pores in the outer ring, e.g. Region I. $S1^{closedII}_{31nm}$: isotherm of the closed bottom pores in Region II. Inset shows the enlargement of their final part close to saturation. $S1^{openII}_{31nm}$: hysteresis loop of the open pores in Region II

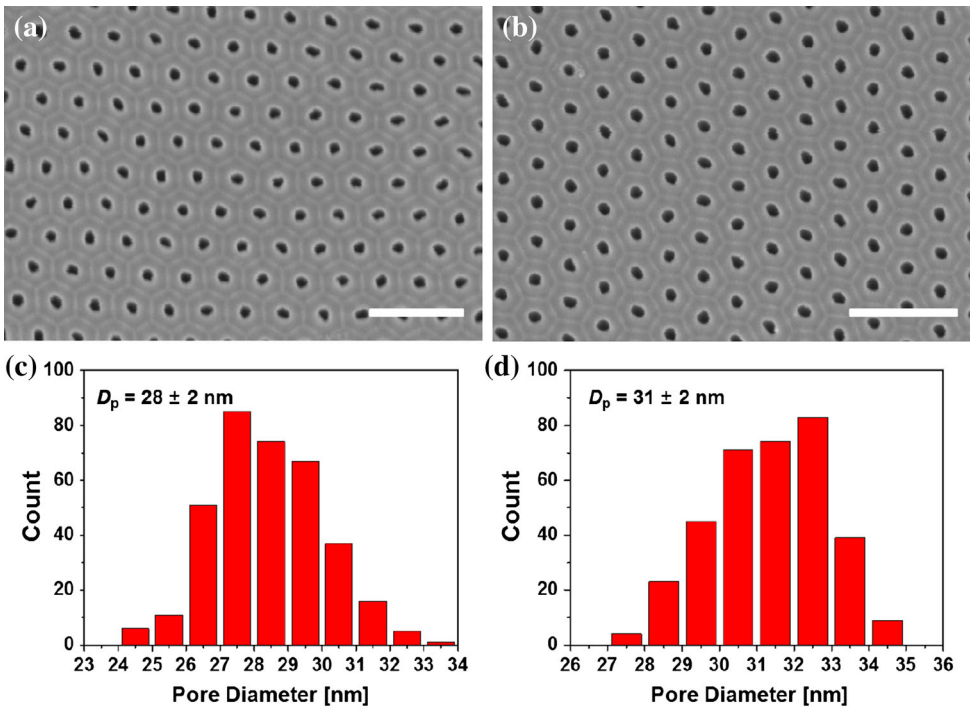

Fig. 7 Representative surface SEM images of **a** the outer ring, Region I, and **b** of the central area, Region II, of porous AAO sample $\mathbf{S1^{bare}_{31nm}}$. The pore size distributions in the respective images are shown as histogram in **c** and **d**. *Scale bars* in (a) and (b) are 250 nm

The difference in the positions of the adsorption branches is instead related to the pore size. To analyze this aspect in more detail, the inset of Fig. 6 shows the normalized isotherms. It clearly appears that the loop of region I is shifted to lower pressures than the corresponding one of region II. If we analyze the desorption branches in terms of Eq. 1, we get $D_p = 25 \pm 4$ nm ($P_{mid\text{-}point}/P_0 = 0.917$) for the pores in the outer ring and $D_p = 27 \pm 3$ nm ($P_{mid\text{-}point}/P_0 = 0.925$) for those in the central region. A similar difference between the size of the pores in the two regions has been observed with electron micrography. Figure 7 summarizes the results of SEM real space analysis of pore sizes which yield $D_p = 28 \pm 2$ nm in the outer ring and $D_p = 31 \pm 2$ nm. This small difference in pore size can be attributed to the slight etching of the pore wall oxide in the central region upon opening of the barrier oxide layer.

Although we can detect the pore opening point and stop the barrier layer removal process, slight pore widening by the infiltrated etching solution is inevitable.

In the inset of Fig. 6 we have also added the normalized isotherm S_{31nm}^{openII} corresponding to adsorption on the open pores of region II. For this pore size, blocking one end of the pores has a small effect on the adsorption loops: the adsorption branches coincide, while the evaporation branches slightly differ. In particular, the loops of the closed pores are a little wider than those of the corresponding open pores. This behavior confirms that found on smaller pores with $D_P = 22$ nm, which was explained in terms of quenched disorder of the pore matrix (Bruschiet al. 2014): the pores sections are not constant along their axes and the pore filling and emptying is driven by the smallest constrictions of the pores regardless of the pore openings (Bruschi et al. 2010).

The fact that the size of the pores does not change significantly between the center and the outer ring explains why the isotherm on the bare sample does not show the two subloops of Fig. 3. Actually, the S_{31nm}^{bare} isotherm can be considered as the convolution of the $S_{31nm}^{closedI}$ and S_{31nm}^{openII} isotherms and the resulting hysteresis loop lies somewhere between those of the two regions.

4 Conclusions

We have measured the adsorption of Ar on mesoporous alumina membranes having straight pores of nominal size $D_p = 83$ nm and $D_p = 31$ nm in their central area. The samples have been prepared by anodization and great attention has been paid to the proper opening of the barrier oxide layer and also widening of pores. Adsorption isotherms taken with a torsional microbalance on the large pores samples ($D_p = 83$ nm) show two distinct hysteresis loops. Detailed measurements performed by selectively blocking pores in different regions allow to conclude that the closed bottom pores in the outer ring (Region I) are smaller than the open pores in the central area of the sample (Region II). This interpretation is confirmed by extensive SEM investigations on the samples and it is likely a consequence of the etching process used to open the barrier layer and widen the pores. Instead, the adsorption isotherm on the small pores ($D_p = 31$ nm) presents the standard single loop expected for straight, non-interconnected pores. A detailed analysis of the contributions of the different sample areas indicate that also in this case the closed bottom pores in the outer ring are slightly smaller than the open pores in the central sample area. However, the small difference between these pores, on the order of 2 nm, is not sufficient to produce two distinct loops. More generally, this study shows how powerful adsorption isotherms are in the analysis of the pore morphology of samples with extended areas and that, at least for this kind of regular porous matrices, the simple analysis of the adsorption isotherms based on the classical Kelvin equation provide results which are in good quantitative agreement (around 10 %) with those obtained by SEM real space analysis.

Acknowledgments This work is supported by KRISS project "Anodization Research Laboratory (KRISS-2013-13011082)".

References

Asefa, T., MacLachlan, M.J., Coombs, N., Ozin, G.A.: Periodic mesoporous organosilicas with organic groups inside the channel walls. Nat. Nanotechnol. **402**, 867–871 (1999)

Bang, J., Kim, S.H., Drockenmuller, E., Misner, M.J., Russell, T.P., Hawker, C.J.: Defect-free nanoporous thin films from ABC triblock copolymers. J. Am. Chem. Soc. **128**, 7622–7629 (2006)

Beck, J.S., Vartuli, J.C., Roth, W.J., Leonowicz, M.E., Kresge, C.T., Schmitt, K.D., Chu, C.T.W., Olson, D.H., Sheppard, E.W.: A new family of mesoporous molecular sieves prepared with liquid crystal templates. J. Am. Chem. Soc. **114**, 10834–10843 (1992)

Bruschi, L., Mistura, G., Park, S. J., Lee, W., Do, D.D.: Adsorption on alumina pores open at one and at both ends (2014, submitted)

Bruschi, L., Mistura, G.: Adsorption within and on regularly patterned substrates. J. Low Temp. Phys. **157**, 206–220 (2009)

Bruschi, L., Carlin, A., Mistura, G.: Wetting on a geometrically structured substrate. J. Chem. Phys. **115**, 6200–6203 (2001)

Bruschi, L., Carlin, A., Parry, A.O., Mistura, G.: Crossover effects in the wetting of adsorbed films in linear wedges. Phys. Rev. E **68**, 021606 (2003)

Bruschi, L., Fois, G., Mistura, G., Sklarek, K., Hillebrand, R., Steinhart, M., Gösele, U.: Adsorption hysteresis in self-ordered nanoporous alumina. Langmuir **24**, 10936–10941 (2008)

Bruschi, L., Mistura, G., Liu, L., Lee, W., Gösele, U., Coasne, B.: Capillary condensation and evaporation in alumina nanopores with controlled modulations. Langmuir **26**, 11894–11898 (2010)

Casanova, F., Chiang, C.E., Li, C.P., Roshchin, I.V., Ruminski, A.M., Sailor, M.J., Schuller, I.K.: Gas aadsorption and capillary condensation in nanoporous alumina films. Nanotechnology **19**, 315709 (2008)

Casanova, F., Chiang, C.E., Ruminski, A.M., Sailor, M.J., Schuller, I.K.: Controlling the role of nanopore morphology in capillary condensation. Langmuir **28**, 6832–6838 (2012)

Esparza, J.M., Ojeda, M.L., Campero, A., Dominguez, A., Kornhauser, I., Rojas, F., Vidales, A.M., Lopez, R.H., Zgrablich, G.: N_2 sorption scanning behavior of SBA–15 porous substrates. Colloids Surf. A **241**, 35–45 (2004)

Evans, R., Marconi, U.M.B., Tarazona, P.: Capillary condensation and adsorption in cylindrical and slit–like pores. J. Chem. Soc. Faraday Trans. **82**, 1763–1787 (1986)

Everett, D.H.: In: Flood, E. A. (ed.) The Solid Gas Interface, vol. 2. Marcel Dekker, New York (1967)

Fan, C., Do, D.D., Nicholson, D.: On the existence of a hysteresis loop in open and closed end pores. Mol. Simul. (2014). doi:10.1080/08927022.2013.869805

Gelb, L.D.: The Ins and Outs of Capillary Condensation in Cylindrical Pores. Mol. Phys. **100**, 2049–2057 (2002)

Gregg, S.J., Sing, K.S.W.: Adsorption, Surface Area and Porosity. Academic Press, New York (1982)

Grosman, A., Ortega, C.: Nature of capillary condensation and evaporation processes in ordered porous materials. Langmuir **21**, 10515–10521 (2005)

Grosmann, A., Ortega, C.: Cavitation in metastable fluids confined to linear mesopores. Langmuir **27**, 2364–2374 (2011)

Han, H., Park, S.J., Jang, J.S., Ryu, H., Kim, K.J., Baik, S., Lee, W.: In situ determination of the pore opening point during wet–chemical etching of the barrier layer of porous anodic aluminum oxide: nonuniform impurity distribution in anodic oxide. ACS Appl. Mater. Interfaces **5**, 3441–3448 (2013)

Hoa, M.L.K., Lu, M., Zhang, Y.: Preparation of porous materials with ordered hole structure. Adv. Colloid. Interface. Sci. **121**, 9–23 (2006)

Kruk, M., Jaroniec, M.: Gas adsorption characterization of ordered organic-inorganic nanocomposite materials. Chem. Mater. **13**, 3169–3183 (2011)

Kruk, M., Jaroniec, M., Ko, C.H., Ryoo, R.: Characterization of the Porous Structure of SBA–15. Chem. Mater. **12**, 1961–1968 (2000)

Lee, W., Kim, J.C.: Highly ordered porous alumina with tailor-made pore structures fabricated by pulse anodization. Nanotechnology **21**, 485304 (2010)

Lee, W., Park, S.-J.: Porous anodic aluminum oxide: anodization and templated synthesis of functional nanostructures. Chem. Rev. **114**, 7487–7556 (2014)

Lee, W., Ji, R., Gösele, U., Nielsch, K.: Fast fabrication of long-range ordered porous alumina membranes by hard anodization. Nat. Mater. **5**, 741–747 (2006)

Lee, W., Han, H., Lotnyk, A., Schubert, M.A., Senz, S., Alexe, M., Hesse, D., Baik, S., Gösele, U.: Individually addressable epitaxial ferroelectric nanocapacitor arrays with near Tb Inch^{-2} density. Nat. Nanotechnol. **3**, 402–407 (2008a)

Lee, W., Schwirn, K., Steinhart, M., Pippel, E., Scholz, R., Gösele, U.: Structural engineering of nanoporous anodic aluminum oxide by pulse anodization of aluminum. Nat. Nanotechnol. **3**, 234–239 (2008b)

Marconi, U.B.M., van Swol, F.: Microscopic model for hysteresis and phase equilibria of fluids confined between parallel plates. Phys. Rev. A **39**, 4109–4116 (1989)

Masuda, H., Fukuda, K.: Ordered metal nanohole arrays made by a two-step replication of honeycomb structures of anodic alumina. Science **268**, 1466–1468 (1995)

Mistura, G., Pozzato, A., Bruschi, L., Grenci, M., Tormen, M.: Continuous adsorption in highly ordered porous matrices made by nanolithography. Nat. Commun. **4**, 2966 (2013)

Morishige, K., Ito, M.: Capillary condensation of nitrogen in MCM–41 and SBA–15. J. Chem. Phys. **117**, 8036–8041 (2002)

Nguyen, P.T.M., Do, D.D., Nicholson, D.: On the irreversibility of the adsorption isotherm in a closed–end pore. Langmuir **29**, 2927–2934 (2013)

Rasband, W.: Image J, released 1.36b; NIH: USA, 2006. (public domain, http://reb.info.nih.gov/ij/)

Rascón, C., Parry, A.O., Nürnberg, R., Pozzato, A., Tormen, M., Bruschi, L., Mistura, G.: The order of condensation in capillary grooves. J. Phys.: Condens. Matter **25**, 192101 (2013)

Sarkisov, L., Monson, P.A.: Modeling of adsorption and desorption in pores of simple geometry using molecular dynamics. Langmuir **17**, 7600–7604 (2001)

Sing, K.S.W., Everett, D.H., Haul, R.A.W., Moscou, L., Pierotti, R.A., Rouquerol, J., Siemieniewska, T.: Reporting physisorption data for gas/solid systems with special reference to the determination of surface area and porosity. Pure Appl. Chem. **57**, 603–619 (1985)

Stein, A.: Sphere Templating Methods for Periodic Porous Solids. Microporous Mesoporous Mater. **44**, 227–239 (2001)

Stein, A.: Advances in microporous and mesoporous solids—highlights of recent progress. Adv. Mater. **15**, 763–775 (2003)

Xia, Y., Rogers, J.A., Paul, K.E., Whitesides, G.M.: Unconventional methods for fabricating and patterning nanostructures. Chem. Rev. **99**, 1823–1848 (1999)

Xia, Y., Gates, B., Yin, Y., Lu, Y.: Monodispersed colloidal spheres: old materials with new applications. Adv. Mater. **12**, 693–713 (2000)

Ying, J.Y., Mehnert, C.P., Wong, M.S.: Synthesis and applications of supramolecular-templated mesoporous materials. Angew. Chem. Int. Ed. **38**, 56–77 (1998)

Zakhidov, A.A., Baughman, R.H., Iqbal, Z., Cui, C., Khayrullin, I., Dantas, S.O., Marti, J., Ralchenko, V.G.: Carbon structures with three-dimensional periodicity at optical wavelengths. Science **282**, 897–901 (1998)

Zhao, D.Y., Feng, J.L., Huo, Q.S., Melosh, N., Fredrickson, G.H., Chmelka, B.F., Stucky, G.D.: Triblock copolymer syntheses of mesoporous silica with periodic 50 to 300 angstrom pores. Science **279**, 548–552 (1998a)

Zhao, D.Y., Huo, Q.S., Feng, J.L., Chmelka, B.F., Stucky, G.D.: Nonionic triblock and star diblock copolymer and oligomeric surfactant syntheses of highly ordered, hydrothermally stable, mesoporous silica structures. J. Am. Chem. Soc. **120**, 6024–6036 (1998b)